Workshop on Visualisation in Environmental Sciences (EnvirVis) (2022)
S. Dutta and K. Feige and K. Rink and D. Zeckzer (Editors)

LiDAR Operation and Digital Modeling Visualization to Communicate Stormwater Management at Green Spaces in Developing Regions

C.-Y. Lin[†1] A. Ackerman[1] D. Johnston[1] G. Tian[2] and Y. Liu[2‡]

[1]Department of Landscape Architecture, SUNY College of Environmental Science and Forestry, Syracuse, USA
[2]College of Landscape Architecture and Art, Henan Agricultural University, Zhengzhou, China

Abstract

This research involves the application of LiDAR modifications from China Meteorological Data Service Centre (CMDC) along with landscape digital modeling visualization tools to explore future climate change adaptation, potential landscape performance and strategic management at the Green Expo Park in Zhengzhou, China. In terms of yearly and numerical reports of weather conditions by CMDC, patterns of runoff distribution and detentions are highly correlated with leaf area index (LAI) and associated factors such as ground materials and physical characteristic. This observation is valuable as environmental inspection for stormwater management at green spaces in developing regions and further understanding of collaboration for landscape architects, urban designers, urban planners, stakeholders and government agencies. Using a combination of a LiDAR360 along with terrain 3D modeling and parametric plugin software, we visualized several surface flow scenarios which were used to potentially inform land of recreation, green spaces and water quality management. Data collected from a LiBackpack 50 instrument was selected for initial reference and processed in LiDAR360, after which point the data was exported for 3D modeling. Parametric plugins were used to develop data supported computational simulation in order to visualize runoff dispersal and aggregation that occurred as a result of various site conditions. These visualizations, developed from LiDAR to digital modeling using parametric digital tools, allowed data-driven exploration of stormwater management and climate change.

Keywords: LiDAR, surface flow, LAI, digital modeling, visualization

1. Introduction

A flood, which is a general and temporary condition of partial or complete inundation of two or more acres of normally dry land area, can be induced by overflow of inland or tidal water, mudslides, collapse or subsidence of lands or unusual and rapid accumulation with runoff of surface waters from any source. Mitigation approaches include stormwater management focused particularly in developed areas. For decades, the United States Environmental Protection Agency has worked to reduce runoff and improve water quality by implementing stormwater management at its facilities. Through collaboration with environmental scientists and consultants, engineers, urban planners and designers, and landscape architects, urban development proposals are commonly required to adhere to regulations such as applications of pervious surfaces and grading design on streetscapes. However, flooding issues are regarded as requiring more comprehensive, even radical, mitigation. For example, an extreme rainstorm occurring in mid-July 2021 in Zhengzhou, China, resulted in over three hundred deaths. This tragedy occurred in an area known as a model for floodwater and stormwater management within rapid, high density urban development.

Due to increasing severity of extreme weather events, innovative landscape designs have become more common as a way of proactively addressing potential flooding due to rainfall. Patterns of the scale, pace, and intensity of human activity on the earth is fundamentally impacting our climate system. We are living in what has been described as the 'Anthropocene Epoch', characterized by rapid human-driven alterations of earth's natural patterns on a global scale. Based on pathways to a 'good' Anthropocene, radical changes to our physical environment require more holistic, intertwined social-ecological-technological systems understanding and approaches [MMRG*21]. In rethinking these systems, we can harness the power of data combined with illustrative visualization

† PhD Candidate at SUNY ESF. Email address: clin16@syr.edu
‡ Corresponding author. Email address: liuyang1991@henau.edu.cn

DOI: 10.2312/envirvis.20221056

which can help us to prioritize and develop novel strategies in design and planning practice.

While most collected environmental data is typically organized in a two-dimensional matrix format, environmental and spatial researchers and analysts have developed technological tools for transforming this data into three-dimensional format for analysis and visualization. There are examples of collaboration between environmental data science and landscape 3D modeling analysis in Leadership in Energy and Environmental Design (LEED) projects in order to better understand financial and environmental quality considerations [CST16], as well as efforts to improve precision in terrain data for computational simulation [LLC20]. It is now common to perform complex, visually realistic urban flood simulations using a variety of computational solvers to accurately model surface water flow. One effective example exploring flood management in sponge cities in China, models surface runoff and integrates characteristics of land use calculation including both residential and vehicular land use types as well as bare land, forest land, and grassland resulting in a 3D model that can be experienced in virtual reality [WHM*19]. Other approaches include hydrological modeling of landscape flooding using ESRI ArcGIS and Autodesk Civil 3D to model detailed street and gutter conditions and derive topography, land cover, soil permeability, and infrastructure from LiDAR data [HC14]. Tree canopy point clouds have been used to calculate free throughfall to understand the impact of trees on rainfall storage and measuring metrics of ecosystem services [BLGP*18]. Researchers have even computationally calculated complex interactions between trees and rain using real-time game engines to improve realism of rainy scenes [WJG*16]. Each of these visualization examples address important uses of data to effectively convey the scientific realities of stormwater in the landscape, often using powerful visualization techniques. Yet it is critical to be able to visualize both surface stormwater conditions as well as the impact of tree canopy on rain storage and infiltration. Our research aims to account for these numerous interrelated aspects of rainfall in the landscape to produce reliable simulations of site and sub-site runoff and catchment.

Making climate change data visual is critically important in communicating findings to experts as well as general audiences [HLSC16]. Climate change visualizations are influential tools in conveying concerning data and can be considered both communicative as well as political in nature [Sch12]. These types of visualizations which higlight local effects can be useful in creating engagement with the public [She15]. Research suggests that distant images of climate change omit human elements, whereas encouraging human experiences and scales can promoite deeper engagement [WCCM18]. Cognitive constraints connected to risk perception can hold individuals back from taking action towards mitigating climate change; visualizations have the potential to overcome this paralysis by providing approachable information to the public [GBNL17].

The goal of our research is to apply LiDAR collection and computational modeling to investigate how digital technology adoption in design and planning practice can enable analysis of urban green space management. Our initial research application took place at Green Expo Park in Zhengzhou, which suffers from extreme storms and flooding caused by climate change in 2021, in order to experiment and understand stormwater management within urban green spaces. We aim to identify the landscape factors which primarily mitigate stormwater surface flow and catchment. This research is supported by the Green Expo Park and the Henan province in China, which enables us to maintain a strong connection with site management personnel who allow ongoing access to the site for research purposes.

The research takes the form of a case study of stormwater runoff visualization applied to a LiDAR dataset which includes terrain and tree canopy information. Our research approach attempts to visualize surface flow distribution and water detention associated with factors calculated using a hydrological formula which calculates the relationship between leaf area index (LAI) and surface flow in urban green spaces. Our stormwater visualizations focus on the Green Expo Park in Zhengzhou, China (Figure 1). The simulated weather conditions use a typical rainfall amount occurring over an hour of rainfall. This time period represents a standard duration of rainfall appropriate for a comprehensive simulation without becoming computationally burdensome. Our workflow (Figure 2) begins with the acquisition of a LiDAR point cloud as the spatial basis for creating a sequence of runoff progressions which reveal relationships between surface water flow and LAI. The resulting visualizations can open up investigation, engagement, and communication of radical landscape change as part of a larger shift towards a 'good' Anthropocene. Moreover, a seamless and dynamic workflow which incorporates parametric visualization allows us to test simulation of future conditions while maintaining control over multiple variables. Compared with a traditional 2D map-based visualization, 3D simulation generated from a real-time LiDAR dataset allows us to communicate spatial qualities of the simulation to a broad audience regardless of prior knowledge or qualifications, enabling this audience to envision themselves in the setting being shown.

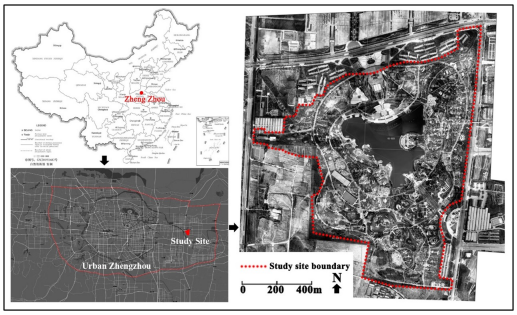

Figure 1: *Location and the boundary of the study area*

2. Methodology

2.1. Data Collection and Operation in LiDAR360

2.1.1. Data Source (LiDAR Collection)

LiDAR point cloud data was collected by Beijing Digital Green Earth Technology Co., Ltd. using a LiBackpack 50 LiDAR device, which relies on a VLP16 sensor of a scanning accuracy of ± 3 centimeters. The sensor's Vertical viewshed angle ranges from

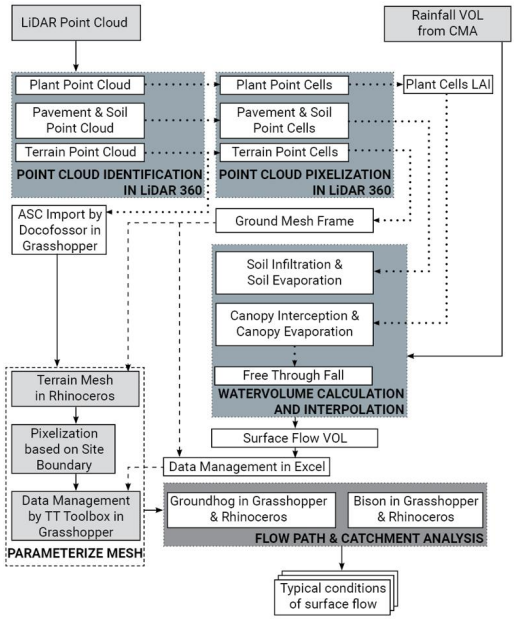

Figure 2: *The workflow from LiDAR point cloud to digital modeling simulation and typical observations*

between -15 to 15 degrees, with a measurement range of 100 meters.

2.1.2. Research Methodology and Data types

In order to prepare the collected data for computational simulation, the collected LiDAR point cloud was processed using LiDAR360 (Figure 3), a comprehensive point cloud post-processing software. In LiDAR360, we applied a default function known as pixelization in order to divide the site into smaller areas. The pixelized plots were set to 15x15 meter sections, a standard size suggested by LiDAR360in order to prevent demotion of tree crowns while retaining precise Leaf Area Index (LAI) values. Pixelizing the site enabled us to account for sitewide variation in detailed factors related to rainfall canopy interception, surface infiltration and evaporation. We adjusted values for vegetation coverage and corresponding LAI within each smaller site area, and adjusted values for two major surface materials: soft pervious and hard impervious. By first fine-tuning values for vegetation coverage, LAI, and surface materials, and then combining the pixelized areas into a model of the entire site, we were able to calculate detailed surface runoff volumes throughout the entire site for use in visual analysis. We exported this information as Tiff files which included LAI and surface material information. A supplementary CSV file was also exported to be used for data analysis and runoff calculations.

2.1.3. Data Organization and Verification in LiDAR360

The LiDAR point cloud was collected during the leaf-on period between June and August 2020 and divided into 23 smaller areas for further processing. To eliminate unusable digital noise, we manually performed between four and six calibrations in each of the 23

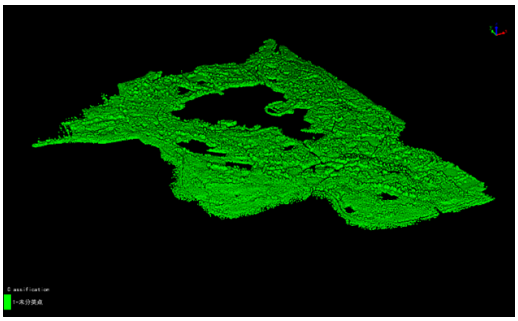

Figure 3: *Data collected, organized and visualized in LiDAR360*

smaller areas to increase the point clouds' accuracy. We then ran each point cloud through several calculations [LT15] (Equation 1-2) first for further denoising and then for normalization to remove inaccurate data points.

$$MaxD = medianD + meanK \times \sigma \tag{1}$$

where:
Equation 1 represents the formula of denoising.
D = The average distance between specified neighborhood points and each data point;
$medianD$ = The median of D;
σ = The standard deviation of D;
K = A multiple of $\sigma whichvalue5isoftenassigned$;
If D>MaxD, a data point is recognized as a noise point.

$$Zi_{norm} = Zi - Zi^{dem} \tag{2}$$

where:
Equation 2 represents the formula of normalization.
Zi_{norm} = The normalized Z value of each data point above the ground;
Zi = The Z value of each data point above the ground which is value 0;
$Zidem$ = A corresponding value of projected data point generated as a digital elevation model (DEM) by an ordinary kriging method at a 0.2 meters resolution [GLYA10].

2.1.4. Data Classification and Preparation for Digital Modeling Simulation

Classification identifies differences in point cloud objects and groups them by similar features. We used LiDAR360 to classify and distinguish four types of point cloud data: bare ground, impervious pavement, buildings and other structures, and vegetation. In order to connect the workflows between LiDAR360 and digital modeling and analysis, we developed a series of mathematical calculations based on a physically-based Urban Forest Effects-Hydrology (UFORE-Hydro) model. This mathematical calculation is regarded as an essential formula for translating collected data and related environmental factors into surface flow values for use in further computational simulation. The UFORE-Hydro model primarily considers interception and infiltration effects of tree canopies

during rainfall, as well as accounting for impacts due to soil and evaporation during precipitation. This methodology can generate a precision runoff value in light ($\leq$ 30 millimeters) and medium ($\leq$ 60 millimeters) precipitation, events that occur more frequently in the study site than heavy precipitation. The surface runoff calculation sequence based on the UFORE-Hydro model includes two major parts which account for tree canopy rainfall interception, free throughfall and evaporation, and soil infiltration and evaporation. According to the collected point cloud, the study site contains a very small percentage of hardscape in-situ. This percentage is small enough that we simplified our LAI calculations to reflect previous surface conditions. For the preparation of further digital modeling simulations, we decide to leave LAI as an independent variable while setting other variables as dependent. This allowed us to focus on the relationship between LAI and surface flow (Equation 3-11) [Dea78] [NP89] [Bev84].

$$S = S_L LAI - \alpha(S_L LAI) \tag{3}$$

where:
Equation 3 represents the formula of considering canopy interception, evaporation and free throughfall.
S = The storage capacity equal to the maximum of C (C_{max}) of the forest canopy as linearly related to LAI [SGX*20];
S_L = A coefficient of specific leaf storage which is 0.2mm in UFORE-Hydro;
α = The LAI adjusted coefficient : $0.00008P^2 - 0.0123P + 781$ (November to April) ; 0 (May to October).

$$E_c = (\frac{C}{S})^{\frac{2}{3}} E_p,\ C < S \parallel E_p,\ C \geq S \tag{4}$$

where:
Equation 4 represents the formula of detailed consideration for canopy evaporation referenced from [Dea78] and [NP89].
$E_c(mm)$ = The value of the canopy evaporation;
E_p = The potential evaporation coefficient of the canopy that is 0.2mm/h described as the average evaporation potentials of trees and shrubs by modified Penman-Monteith equation [Sta93];
When P, the precipitation, is greater than S (C - S), the overload precipitation will be recognized as the free throughfall to the ground and not participation into the canopy evaporation. C represents canopy areas.

$$P_f = 0,\ P < (S + E_c) \parallel P - (S + E_c),\ P \geq (S + E_c) \tag{5}$$

where:
Equation 5 represents the formula of detailed consideration for free throughfall.
P_f = The second stage, defined by the UFORE-Hydro model, when stored rain equals S with no further interception and all subsequent precipitation reaches the ground.

$$I_r = C_w K_s (\frac{h + S_m}{Z} + 1) \tag{6}$$

where:
Equation 6 represents the formula of considering soil infiltration, evaporation, and surface runoff.
I_r = The steady soil infiltration rate;
C_w = The hydraulic conductivity coefficient, 0.95 as sandy soil from the experimental result [WGC*20];
K_s = The saturated hydraulic conductivity of upper layer soil, numbered as 1.5mm/s. h.;
h = The pressure head (h) in 30mm.;
S_m = The average water entry suction (S_m)in3.12.;
Z = The depth of sandy layer, numbered as 250mm based on the site survey.

$$Q_o = 0\ (P_f < \Delta t I_r) \parallel P_f - \Delta t I_r\ (P_f \geq \Delta t I_r) \tag{7}$$

where:
Equation 7 represents the formula of over-infiltration surface within steady infiltration rate.
The period of time (Δt) is $\Delta t I_r(mm)$;
Q_o = The result of over-infiltration surface runoff when P_f is greater than C_i

$$S_i = (S_s - \omega) P_b \tag{8}$$

where:
Equation 8 represents the formula of detailed consideration for soil storage capacity.
S_i = Water storage which is a dynamic value;
S_s = Soil saturated moisture capacity as 336.25g/kg in average depth of 100cm soil cover;
ω = Field moisture capacity as 305.05g/kg in average depth of 100cm soil cover;
P_b = soil bulk density in 1.42g/cm^3.

$$E_i = (\frac{C_i}{S_i})\ E_{rc},\ C_i < S_i \parallel E_{rc},\ C_i \geq S_i \tag{9}$$

where:
Equation 9 represents the formula of detailed consideration for soil evaporation.
E_i = The site evaporation value;
E_rc = The soil evaporation rate for the referenced planting type, valued as 0.35mm/h for the herb ground cover area;
C_i = The soil infiltration amount.

$$Q_s = 0\ (\Delta t I_r < (S_i + E_i)) \parallel \Delta t I_r - (S_i + E_i)\ (\Delta t I_r \geq (S_i + E_i)) \tag{10}$$

where:
Equation 10 represents the formula of over-storage surface within steady infiltration rate.
Q_s = The over-storage surface runoff when C_i is greater than S_i.

$$Q_r = Q_s + Q_o \tag{11}$$

where:
Equation 10 represents the formula of the sum of runoff.
Q_r = The sum of over-infiltration and over-storage runoff.

2.2. Parametric Analysis in Digital Modeling Simulation

2.2.1. Generation of Site Terrain Mesh

To begin 3D modeling and spatial analysis while maintaining flexibility, we decided to use 3D modeling software, Rhinoceros, and its parametric interface, Grasshopper. First we generated the topography by importing the Action Script Communication (ASC) file which was generated by LiDAR360 from the collected point cloud. To generate a topographic mesh surface from the ASC file, we used Docofossor, a Grasshopper plugin, to extract ASC file point elevation values and place them at their corresponding elevations within the Rhino 3D modeling environment. In order to avoid computational overload, we trimmed the mesh surface using another Grasshopper plugin, Pufferfish, to reduce the mesh terrain down to the limits of Zhengzhou Green Expo Park (Figure 4).

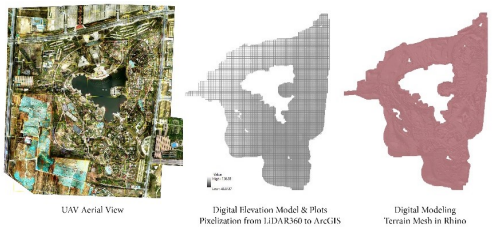

Figure 4: *Transformation from LiDAR collection through asc. file to terrain mesh in digital modeling*

2.2.2. Customized Pixelization

Because we used LiDAR360 to divide the entire site into 15x15 meter pixels to calculate LAI and other attributes such as surface materials and soil properties on smaller sections of the site, we needed to also develop a method of applying these attributes to specific sections of the site. To do this, we developed a Grasshopper script to associate the attributes to each pixelated section of the site. This involved building a 225-square meter grid on top of the terrain mesh which outlined each individual 15x15 meter pixel across the entire site. With the grid in place, we linked the dataset from LiDAR360 and arranged the index order to assign corresponding attributes to each pixel.

2.2.3. Cohesive Data Implementation

While data exported from LiDAR360 is compatible with multiple other file formats, the structure of the exported data proved challenging to import to the Grasshopper interface. Instead of trying to connect the LiDAR360 data directly into Grasshopper, we used Microsoft Excel as an intermediary between the two programs. This was accomplished by using another Grasshopper plugin named TT Toolbox to link our external CSV file directly into Grasshopper. After successfully linking the CSV into Grasshopper, we were able to use the 225-square meter grid to adjust computational rainfall to reflect the specific site conditions within each pixel. Each pixel acquired specific LAI information via the CSV file, which then was used to reduce the amount of rainfall particles dropped onto the terrain mesh. Based on a standard drop volume [Gle06], each representative rainfall group contained ten million drops which were compressed and simplified to avoid computational overload.

2.2.4. Flow Calculation and Visualization

To perform runoff visualization, we used three types of flow visualization components within two Grasshopper plugins, Bison and Groundhog (Figure 5). Bison is a landscape architecture plugin for Grasshopper which focuses on a continuous workflow from terrain mesh analysis to editing, and works to keep components concise and intuitive. Developed by Philip Belesky, Groundhog contains a number of components for modeling features within a parametric design process. By means of three types of flow visualization, we aimed to understand surface flow distribution and water detention associated with factors identified by hydrological formulas and calculations, as well as visualizing the relationship between LAI and surface flow in urban green spaces.

We first used the Flow component in Bison to define the boundary for surface flow analysis and correlate these boundaries with the pixel size for rainfall groups falling onto the mesh terrain of the site. The Flow component allowed us to graphically visualize surface flow distribution as impacted by presence of site vegetation and their corresponding LAI.

Next, we used the Flow Simulation and Flow Catchments components in Groundhog. Together, these two components create a collection of pre-calculated flow paths to identify different catchment areas. They also classify each flow path into groups depending upon which paths finish or drain into same approximate location. Furthermore, each catchment type is assigned a volume figure that represents the proportion of flow paths that end within the catchment. This numeric value gives flexibility of further calculation of volumetric load of the whole surface flow associated with LAI in urban green spaces.

Lastly, we used the FlowPath component in Groundhog to visualize projections of overland surface waterflow. With this visualization, we were able to further identify proposed regions with their corresponding representative proportions of catchment areas. Different from Flow component in Bison, the Flows component in Groundhog creates basic simulations which illustrate proposed areas of catchments. However, since it uses hypothetical regions based on random seeds of drop points on the site terrain mesh, we suggest using both flow visualizations to create a holistic understanding of both flow path distribution and catchment impacted by site vegetation and LAI.

It is important to note that Groundhog is a very limited form of catchment/watershed/basin identification, as the flow paths only measure the effects of topography on surface water flow and ignores other important hydrological factors. We recognize that it would be problematic to rely solely on Groundhog to produce flow and catchment simulations that have even general accuracy. To address this, we have performed the majority of our surface flow simulation first by performing calculations with UFORE-Hydro equations to account for tree canopy, surface materials, soils, and evaporation. We then used Grasshopper to connect the results of these calculations with Groundhog's visualization features to visualize the surface flow and catchment scenarios generated through mathematical calculations.

Figure 5: *The parametric definition of runoff visualization*

3. Results

3.1. Surface Flow Distribution

While comparing surface flow distribution between considerations of LAI and other dependent variables, we visualized those areas with greater rainfall interception. The amount and direction of the simplified rainfall group within each pixel represented an overall visualization of the surface flow conditions throughout the site as impacted by variations in LAI. To validate these simulations, overlaid the rainfall visualization with aerial orthoimagery collected by unmanned aerial vehicles (UAV). We inspected the visualizations of areas which appeared to have a high level of rainfall interception, and found that those areas were covered by denser vegetation in aerial images. The comparison of surface flow distribution generated discussion about species and types of clusters of plants that can impactfully increase rainfall storage leading to reduced runoff. To prepare for next steps in evaluating sections of the site at a smaller scale, we created a enlarged viewport to explore the relationship between vegetation characteristics and surface runoff and compare this with surface runoff on bare ground with minimal vegetation (Figure 6).

3.2. Surface Flow Catchment

We applied the same methodology of overlaying exported images to visually compare variations in surface flow catchment due to LAI and other dependent variables. Based on the comparisons, we identified potential areas of flow catchment in less dense vegetated areas. The comparison of surface flow distribution generated an ensuing discussion about the relationship between utilities and topography that effectively support surface water storage. This also generated a subsequent discussion of pavement material implementation. We used a second enlarged viewport to further understand the relationship between hardscape materials in the built environment and surface flow detention and catchment compared to bare ground with minimal vegetation (Figure 7).

3.3. Relationship between Runoff and LAI

In order to better understand the spatial implications of our analysis, we created visualizations of the site both with and without the impact of LAI on surface flow and catchment volume. For these visualizations, we focused on the smaller section of the site indicated Figure 6. We began by creating rendered perspective views of the smaller site section as viewed from the air, with terrain shown in light green, significant surface vegetation such as trees and shrubs shown in darker green, hardscape shown in gray, and water shown in blue. We used a “pipe along curve” command in Rhino to give the surface flow lines enough thickness to be visible from an aerial view. The resulting images provide a 3D visualization of the difference between surface flow calculations with and without LAI (Figure 8).

While these visualizations enabled understanding of the calculations in 3D, they remained abstract, lacking the character of the actual landscape. To better communicate this landscape character, we imported both Rhino models into Lumion, a 3D visualization and imaging software tool. In Lumion, we assigned realistic grass materials to the terrain, concrete and asphalt materials to the primary circulation paths, omitting the minor circulation routes due to pixelization from the LiDAR data. We also added and translucent reflective water materials to the surface flow and catchment areas. For the visualization of surface flow with LAI, we placed tree models in the locations of the most prominent trees on the site. We did not include every tree present in the site as this would obscure the

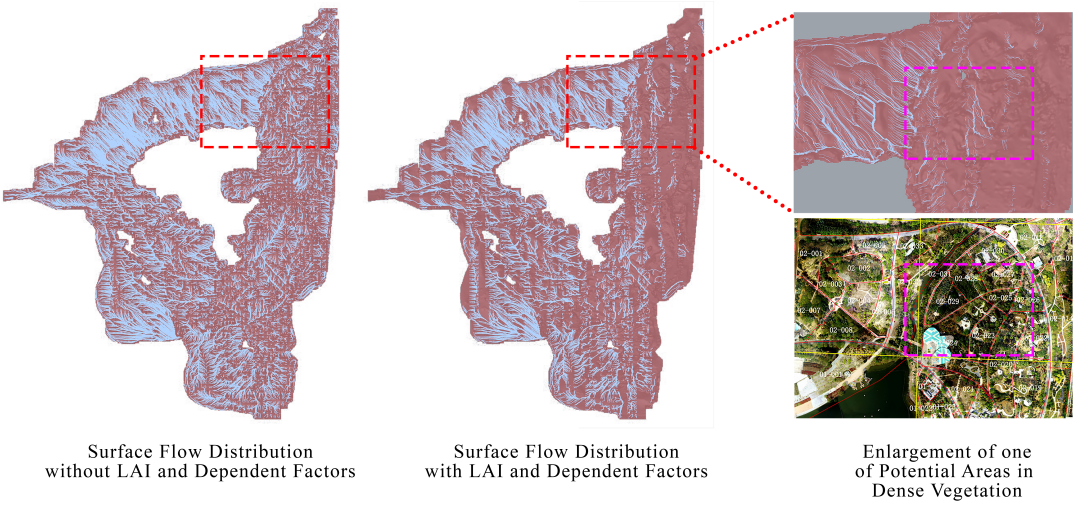

Figure 6: *The comparison of consideration of LAI and dependent factors for surface flow distribution*

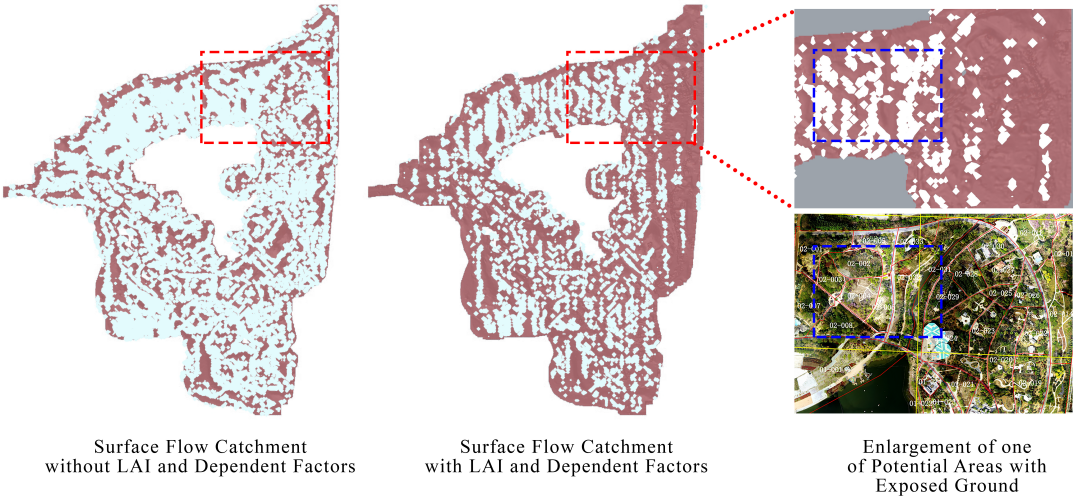

Figure 7: *The comparison of consideration of LAI and dependent factors for surface flow catchment*

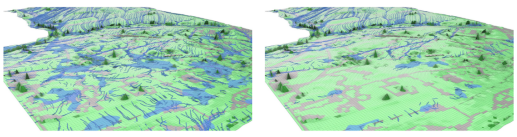

Figure 8: *Rendered aerial visualizations of surface flow and catchment without accounting for LAI (left) and with accounting for LAI (right)*

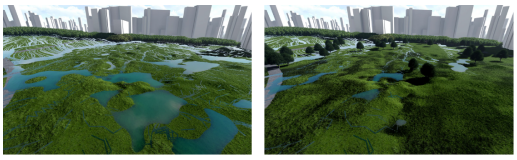

Figure 9: *Realistically rendered aerial visualizations of surface flow and catchment without accounting for LAI (left) and with accounting for LAI (right)*

ability to view the surface hydrology. Instead, we used a dark leafy vegetation material to indicate less prominent vegetation such as shrubs and smaller trees. Lastly, we included background buildings to convey the urban context of the site (Figure 9).

Lastly, we felt it was important to create rendered visualizations of the two different scenarios as seen from the perspective of a person standing on the site. For these visualizations we placed the

viewpoint within the site, lower to the ground as if seen from the eyes of a visitor to the site. We added detailed foreground vegetation, and weather effects to create the impression of a rainstorm. For these visualizations we similarly included trees and other site vegetation in the image showing calculations including LAI. The intent of these visualizations is to allow the viewer to understand the visual and ecological impact of site vegetation on flood mitigation during extreme storm events (Figure 10).

Figure 10: *Immersive first-person perspective view of the site showing surface flow and catchment areas without accounting for LAI (top) and with accounting for LAI (bottom)*

4. Discussions

This data-informed visualization within digital modeling analysis has the potential to clearly and effectively depict the spatial implications of interrelated site conditions beyond simple surface runoff analysis, leading to improved decision-making abilities for land use proposals and project management. We can use these workflows to examine surface flow patterns of the site and illustrate potential areas of detention or retention, allowing us to advocate for the use of landscapes as green infrastructure in urban areas. Furthermore, this type of computational simulation can allow us to infer future flooding patterns which account for changes in stormwater runoff due to presence of vegetation. This can help landscape architects communicate the localized effects of climate change on the landscape and developing regions, using visually accessible tools that can be easily understood by collaborators such as environmental engineers, urban designers and urban planners. By allowing landscape architects to make recorded data visually and spatially explicit, this modeling may also be useful in recreational land management, water quality management, and climate change adaptation. The 3D models that are created with this workflow can be viewed at a human perspective by placing the camera on the ground as if from the vantage point of an observer and a city scale by placing the camera high above the terrain, enabling an overall view of the landscape as if seen from the air. In this research, we use the perspective view to communicate surface water flow as seen from the human scale, whereas we use the aerial top-down view to communicate catchment information which is more applicable to large-scale planning contexts.

As with any simulation, there is likely to be some uncertainty in the results. We cannot claim that these simulations are perfect predictions of what could happen in a current or future situation. However, given our confidence in both the mathematical models as well as the visual simulation tools, we feel that this research reduces the amount of uncertainty compared to simulations which focus solely on water flow and terrain. Our next steps will aim to improve several areas of the research related to accuracy. Both data accuracy and visual realism are essential for the effective use of this workflow in landscape management. A key area to develop in future stages of this research is the refinement of data transition between software and further validation with experiments in-situ of sampling pixelized plots. We are currently conducting further experiments to begin validating our digital simulations by comparing them against real-life measurements of surface flow patterns tested on-site. This process requires data obtained during the rainy season, and must be collected in a continual process over one year. This data collection is currently paused due to COVID-19 restrictions in China. We will continue to monitor changes to these restrictions and will resume data collection when governmental restrictions are lifted.

The use of digital modeling visualization to visualize real-world collected LiDAR data can allow landscape architects to generate dynamic and informative visual media for a range of uses. The workflow is flexible in terms of landscape scale as well as time, allowing the visualization of data across large areas and time periods. Research projects using this workflow can be considered not only as individual site analyses, but also as a case study inventory of stormwater over time which can inform landscape strategies for climate change adaptation.

5. Conclusions

The ability to input collected LiDAR data and and flexibly simulate site conditions using parametric 3D modeling is a beneficial tool to digitally measure and analyze changes to stormwater management over time, whether in single event or in by comparing of multiple flooding possibilities. The additional ability to communicate these changes in an environmental visualization which conveys comprehensive site pavement materials, environmental factors such as interception, infiltration and evaporation, and significant vegetation opens up a wide array of avenues for collaborating with this data. Such collaboration is a critical aspect of modeling and communicating the impacts of climate change. In our research, we propose to understand the capacity of green spaces in mitigating flooding issues at multiple scales, both through digital simulation as well through decision making in design and planning. We believe the digital workflows developed in our research can support increased flexibility for landscape designers and urban planners as they seek to improve their design solutions and simultaneously demystify the complexity of stormwater management. We hope that this workflow – from LiDAR collection to 3D modeling simulation and visualization– can be used to further explore the topic of climate change, flooding issues and stormwater management in the green spaces throughout developing regions.

Acknowledgement

This research is supported by Henan Provincial Joint International Research Laboratory of Landscape Architecture, Zhengzhou Green Expo Park Management Center. It is Funded by: The Key Projects of the Henan Provincial Department of Education (21A220002), The Henan Province Science and Technology Research Project (212102310581).

References

[Bev84] BEVEN K.: Infiltration into a class of vertically non-uniform soils. *Hydrological Sciences Journal 29*, 4 (1984), 425–434. doi:10.1080/02626668409490960. 4

[BLGP*18] BAPTISTA M. D., LIVESLEY S. J., G PARMEHR E., NEAVE M., AMATI M.: Terrestrial laser scanning to predict canopy area metrics, water storage capacity, and throughfall redistribution in small trees. *Remote Sensing 10*, 12 (2018), 1958. doi:10.3390/rs10121958. 2

[CST16] CHEN Y., SAMUELSON H. W., TONG Z.: Integrated design workflow and a new tool for urban rainwater management. *Journal of environmental management 180* (2016), 45–51. doi:10.1016/j.jenvman.2016.04.059. 2

[Dea78] DEARDORFF J. W.: Efficient prediction of ground surface temperature and moisture, with inclusion of a layer of vegetation. *Journal of Geophysical Research: Oceans 83*, C4 (1978), 1889–1903. doi:10.1029/JC083iC04p01889. 4

[GBNL17] GLAAS E., BALLANTYNE A. G., NESET T.-S., LINNÉR B.-O.: Visualization for supporting individual climate change adaptation planning: Assessment of a web-based tool. *Landscape and Urban Planning 158* (2017), 1–11. doi:10.1016/j.landurbplan.2016.09.018. 2

[Gle06] GLEICK P. H.: Water and terrorism. *Water policy 8*, 6 (2006), 481–503. doi:10.2166/wp.2006.035. 5

[GLYA10] GUO Q., LI W., YU H., ALVAREZ O.: Effects of topographic variability and lidar sampling density on several dem interpolation methods. *Photogrammetric Engineering & Remote Sensing 76*, 6 (2010), 701–712. doi:10.14358/PERS.76.6.701. 3

[HC14] HAHN H., CROSS D.: Linking gis-based modelling of stormwater best management practices to 3d visualization. *DLA 2014.–. 647 658* (2014). http://www.semanticscholar.org/paper/Linking-GIS-based-Modeling-of-Stormwater-Best-to-3D-Ha/hn-Cross/0c29a3c981699893f0aa870661395484865ee75e. 2

[HLSC16] HAROLD J., LORENZONI I., SHIPLEY T. F., COVENTRY K. R.: Cognitive and psychological science insights to improve climate change data visualization. *Nature Climate Change 6*, 12 (2016), 1080–1089. doi:10.1038/nclimate3162. 2

[LLC20] LUO J., LEI Z., CAO L.: Visual simulation method of runoff in landscape space based on uav tilt photography. *WIT Transactions on Ecology and the Environment 249* (2020), 363–373. doi:10.2495/SC200301. 2

[LT15] LIU T., TAO D.: Classification with noisy labels by importance reweighting. *IEEE Transactions on pattern analysis and machine intelligence 38*, 3 (2015), 447–461. doi:10.1109/TPAMI.2015.2456899. 3

[MMRG*21] MCPHEARSON T., M RAYMOND C., GULSRUD N., ALBERT C., COLES N., FAGERHOLM N., NAGATSU M., OLAFSSON A. S., SOININEN N., VIERIKKO K.: Radical changes are needed for transformations to a good anthropocene. *Npj Urban Sustainability 1*, 1 (2021), 1–13. doi:10.1038/s42949-021-00017-x. 1

[NP89] NOILHAN J., PLANTON S.: A simple parameterization of land surface processes for meteorological models. *Monthly weather review 117*, 3 (1989), 536–549. doi:10.1175/1520-0493(1989)117<0536:ASPOLS>2.0.CO;2. 4

[Sch12] SCHNEIDER B.: Climate model simulation visualization from a visual studies perspective. *Wiley Interdisciplinary Reviews: Climate Change 3*, 2 (2012), 185–193. doi:10.1002/wcc.162. 2

[SGX*20] SONG P., GUO J., XU E., MAYER A. L., LIU C., HUANG J., TIAN G., KIM G.: Hydrological effects of urban green space on stormwater runoff reduction in luohe, china. *Sustainability 12*, 16 (2020), 6599. doi:10.3390/su12166599. 4

[She15] SHEPPARD S. R.: Making climate change visible: A critical role for landscape professionals. *Landscape and Urban Planning 142* (2015), 95–105. doi:10.1016/j.landurbplan.2015.07.006. 2

[Sta93] STANNARD D. I.: Comparison of penman-monteith, shuttleworth-wallace, and modified priestley-taylor evapotranspiration models for wildland vegetation in semiarid rangeland. *Water Resources Research 29*, 5 (1993), 1379–1392. doi:10.1029/93WR00333. 4

[WCCM18] WANG S., CORNER A., CHAPMAN D., MARKOWITZ E.: Public engagement with climate imagery in a changing digital landscape. *Wiley Interdisciplinary Reviews: Climate Change 9*, 2 (2018), e509. doi:10.1002/wcc.509. 2

[WGC*20] WANG Y., GE L., CHENDI S., WANG H., HAN J., GUO Z., LU Y.: Analysis on hydraulic characteristics of improved sandy soil with soft rock. *Plos one 15*, 1 (2020), e0227957. doi:10.1371/journal.pone.0227957. 4

[WHM*19] WANG C., HOU J., MILLER D., BROWN I., JIANG Y.: Flood risk management in sponge cities: The role of integrated simulation and 3d visualization. *International Journal of Disaster Risk Reduction 39* (2019), 101139. doi:10.1016/j.ijdrr.2019.101139. 2

[WJG*16] WEBER Y., JOLIVET V., GILET G., NANKO K., GHAZANFARPOUR D.: A phenomenological model for throughfall rendering in real-time. In *Computer Graphics Forum* (2016), vol. 35, Wiley Online Library, pp. 13–23. doi:10.1111/cgf.12945. 2